

The Influence of Different Ball-Milling Dispersants on the Structure and Performance of $\text{Li}_3\text{V}_2(\text{PO}_4)_3/\text{C}$ Composites

Zheng Jia, Wenhui Wang, Zheng Liu, Fangna Jia, Rujuan Zheng, Changsong Dai*

School of Chemistry Engineering and Technology, Harbin Institute of Technology, Harbin 150001, China,

*E-mail: changsd@hit.edu.cn.

Received: 1 March 2013 / Accepted: 29 March 2013 / Published: 1 May 2013

The $\text{Li}_3\text{V}_2(\text{PO}_4)_3/\text{C}$ (LVP/C) composite materials have been synthesized with different volume ratio of ethanol and water as ball-milling dispersants. The samples were investigated by X-ray diffraction (XRD), X-ray photoelectron spectroscopy (XPS), scanning electron microscopy (SEM), transmission electron microscopy (TEM) and electrochemical tests. When pure ethanol or water is adopted as ball-milling dispersant, the synthesized LVP/C composite exhibits uniform carbon coating layer with adequate thickness restricting the excessive growth of LVP grains and agglomeration of LVP/C particles, which provides efficient electronic conduction networks as well as good electrochemical reactivity. At 1C rate, the initial discharge capacity of the LVP/C composite synthesized with pure ethanol as dispersant reaches 122.5mAh g^{-1} , which is slightly larger than the sample synthesized with pure water as dispersant (119.6mAh g^{-1}). However, at 10C and 20C rates, both the samples deliver the same initial discharge capacity and cycling stability. The CV and EIS tests show that the lithium-ion diffusion coefficients of the two samples are of the same order of magnitude, indicating that they both have good mass-transport capability.

Keywords: $\text{Li}_3\text{V}_2(\text{PO}_4)_3/\text{C}$ composites, ball milling dispersant, specific capacity, high rate capability, lithium-ion diffusion coefficient.

1. INTRODUCTION

$\text{Li}_3\text{V}_2(\text{PO}_4)_3$ (LVP) has been proposed as one of the most promising cathode materials for power lithium-ion batteries (LIBs) due to its high discharge voltage, high energy density and remarkable thermal stability as well as excellent low-temperature performance [1-4]. However, the three-dimensional frameworks of monoclinic LVP lead to poor electronic conductivity and thus limit high-rate performance [5], therefore carbon coating on LVP surfaces to improve electronic conductivity is a common choice. Many synthesis technologies have been adopted to synthesize the

material [6-10], among which carbon thermal reduction method [11] is the most suitable for industrial production. While the ball milling procedure is the most important step in carbon thermal reduction process because it determines the distributing uniformity of several raw materials and thus the quality of the final product [5, 12-14].

Ethanol was usually employed as dispersing agent of ball milling in most previous researches, but ethanol is expensive and flammable, which makes it a risky factor during the production process, especially for large-scale production. Furthermore, the spraying and drying equipments must have a high explosion-proof capability if ethanol was employed as dispersant during ball milling. In this paper, distilled water was tried to replace at least part of ethanol as ball-milling dispersant so as to reduce the cost and ensure the production safety, and the influence of different ball-milling dispersing agents on the physical and electrochemical properties of the produced LVP/C materials were studied detailedly.

2. EXPERIMENTAL

2.1 Synthesis and characterization of samples

The ball-milling dispersants with volume ratio of ethanol to water ($V_{\text{ethanol}}:V_{\text{water}}$) being 0:1, 1:3, 1:1, 3:1 and 1:0 were prepared in advance. $\text{LiOH}\cdot\text{H}_2\text{O}$ (A.R.), V_2O_5 (A.R.), and $\text{NH}_4\text{H}_2\text{PO}_4$ (A.R.) (molar ratio 3.15: 1.00: 3.00) and a certain amount of sucrose (A.R.) (as carbon source) were put into a planetary ball mill, and then a certain milling dispersant prepared in advance was added, and the mixture was ground for 8h. Then the obtained mixture was pre-heated at 300°C for 4h to expel NH_3 , H_2O and formed the precursor. After cooling, the precursor was carefully ground and then sintered at 800°C for 24h under flowing Ar, and the produced LVP/C composite was ground with an agate mortar.

The morphology of the Samples was observed with a scanning electron microscope (SEM, HITACHI S-4700, Japan) equipped with EDS and a transmission electron microscope (HITACHI H-7650, Japan). X-ray diffraction (XRD) with a powder X-ray diffractometer (Rigaku D/max- γ B, Japan) was performed to identify the crystalline phase of the LVP/C materials with $\text{Cu K}\alpha$ (45kV, 50mA, $\lambda = 0.154178\text{nm}$, step size=0.02°, $10^\circ < 2\theta < 90^\circ$) radiation. X-ray Photoelectron Spectroscopy (XPS) was measured using a PHI5700 ESCA System Spectrometer (Perkin-Elmer, US). The average particle size distributions were determined with .The residual carbon contents of the LVP/C composites were studied using the carbon and sulfur analyzer (TOC-VCN, SHIMADZU SSM-5000A, Japan).

2.2. Assembly of cells and electrochemical measurements

First, 80wt% LVP/C composite, 10wt% carbon black and 10wt% PVDF 1300 were mixed in NMP and stirred for 12h. The obtained slurry was coated on an aluminum foil (the thick was about 20 μm), and dried at 120°C for 12h in a vacuum oven. Then the coated Al foil was compressed under a pressure of 15MPa and punched into 15mm-diameter sheets as cathode plates. The typical weight of the cathode plates were 9~10mg, and the thickness was about 0.1mm. A lithium sheet with 0.30mm

thickness was used as the anode, and Celgard 2400 membrane with 0.02mm thickness as the separator, and 1M LiPF₆ in EC/EMC/DEC (a volume ratio of 1:1:1) as the electrolyte. CR2025-type coin cells were assembled in an argon-filled glove box.

The galvanostatic charge/discharge performances of the cells were tested using a battery testing system (BTS-5V/5mA, Neware company, Shenzhen, China). Cyclic voltammetry (CV) was performed with an electrochemical station (CHI 750d, Chenhua, Shanghai, China) at different scan rates (0.5, 0.3, 0.1 and 0.05mV·s⁻¹) in the range of 3.0~4.3V (vs. Li⁺/Li). The electrochemical impedance spectroscopy (EIS) tests were carried out with a CHI 750d at open circuit potentials with an AC signal of 5mV amplitude over a frequency range from 100kHz to 0.01Hz. Both EIS tests and CV tests were carried out using a two-electrode system of coin-type cell with a LVP/C cathode as working electrode and a lithium sheet as counter electrode and reference electrode. All experiments were carried out at ambient temperature.

3. RESULTS AND DISCUSSION

3.1 Sample characterization

The XRD patterns of the LVP/C composites synthesized with different ball-milling dispersants are shown in Fig. 1. It can be seen that all the diffraction peaks correspond to a single phase of monoclinic LVP with space group $p2_1/n$, which is consistent with the reported in literature [15]. There is no diffraction peak related to carbon, indicating that the residual carbon is amorphous and does not enter the crystal lattice to affect the crystal structure of LVP. The unit-cell parameters are listed in Table 1, from which we can know that these parameters are close to those of LVP phase for all the samples prepared with different dispersants, while the cell volumes for the samples synthesized with pure ethanol or water as dispersant are relatively low implying better structure stability.

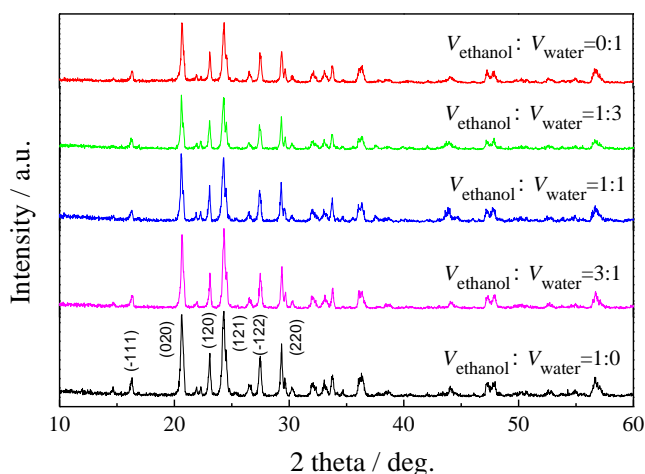


Figure 1. X-ray diffraction patterns of the LVP/C composites synthesized with different ball-milling dispersants

Table 1. Unit-cell parameters and cell volumes of the LVP/C composites synthesized with different ball-milling dispersants

Vethanol:Vwater	<i>a</i> (nm)	<i>b</i> (nm)	<i>c</i> (nm)	β (deg.)	Vol. (nm ³)
0:1	0.860807	0.858794	1.200521	90.2128	0.88749
1:3	0.862553	0.861151	1.216878	91.1279	0.90371
1:1	0.860667	0.86096	1.212854	90.1115	0.89872
3:1	0.853651	0.860618	1.207204	90.0455	0.88689
1:0	0.860669	0.85805	1.194926	90.2791	0.88244

In order to study the effect of the milling dispersants on the element composition and element valence state of the produced precursors and corresponding LVP/C composites, the XPS spectra were measured. Fig. 2 presents the XPS spectra of the LVP/C precursors with pure water (Vethanol:Vwater = 0:1) and ethanol (Vethanol:Vwater = 1:0) as ball-milling dispersants. It can be seen from Fig. 2(a) that the XPS peaks related to V, P, O, C were detected in the two precursors proving the presence of these elements. But since the atomic number of Li is small, it's difficult to distinguish the XPS peaks related to Li in the full XPS spectra. In addition, the valence states of V element in these two precursors are compared in Fig. 2(b). For the precursor produced with pure water (Vethanol:Vwater = 0:1) as ball-milling dispersant, the V2p_{3/2} spectrum comprises two peaks at 517.0eV and 515.7eV, which are close to V₂O₅ (516.9eV) and VO₂ (515.65eV), respectively, and the V2p_{1/2} spectrum has a peak around 523.5eV, corresponding to V element with +4 valence. As to the precursor prepared with pure ethanol (Vethanol:Vwater=1:0) as ball-milling dispersant, the main peak of the V2p_{3/2} spectrum is centered at 517.7 eV, which is attributed to V₂O₅ (516.9 eV), meanwhile, no peak ascribed to V2p_{1/2} is observed. A plausible explanation for the difference in valence state of V element in these two precursors is that the presence of water in place of ethanol promoted the reduction of V₂O₅ by sucrose during the ball milling process.

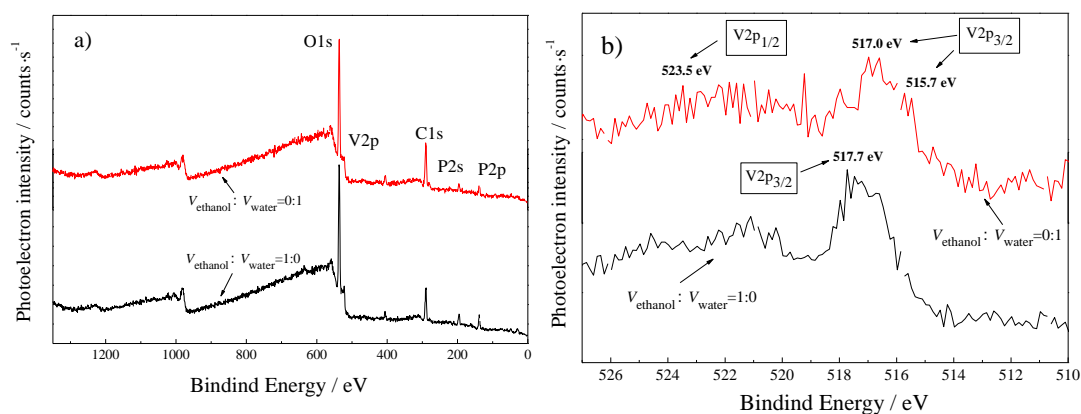
**Figure 2.** Full XPS spectra a) and V2p XPS spectra b) of the LVP/C precursors

Fig. 3 shows that the XPS spectra of the as-synthesized LVP/C products. As can be seen from Fig. 3(b), for the LVP/C materials synthetized using pure water (Vethanol:Vwater=0:1) and ethanol

(Vethanol:Vwater=1:0) as dispersant, the positions of the V2p_{3/2} peak are at 515.5eV and 515.3eV, respectively, all designated to element V with +3 valence. Combining the XPS results in Fig. 2 and 3 we can conclude that, although water as the dispersant used during ball milling may promote the reduction of V⁵⁺ to a certain extent, the final valence state of vanadium ion in the two LVP/C products are all +3.

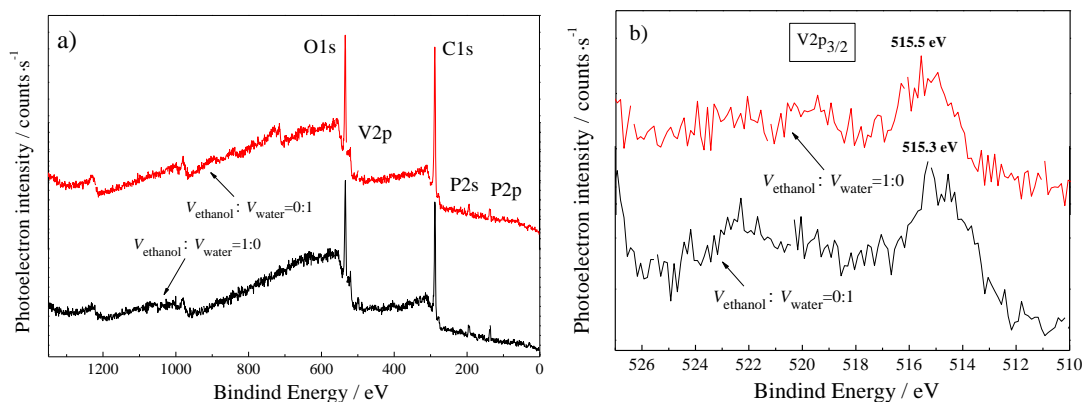
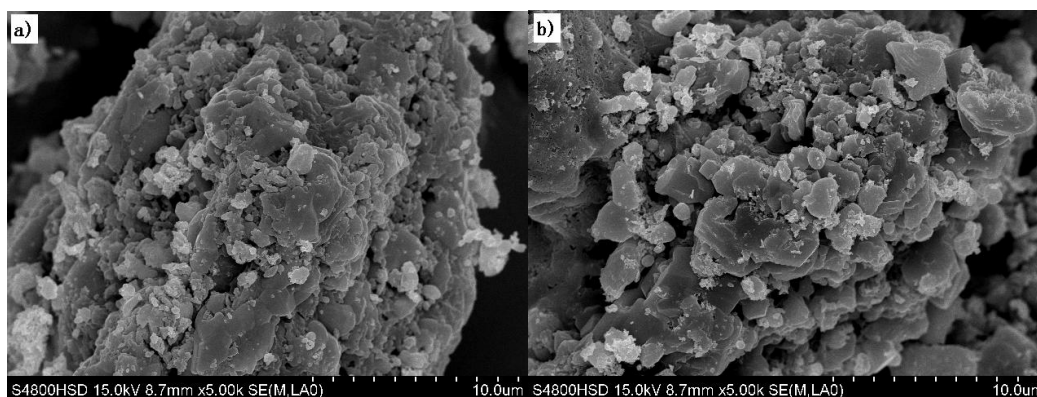


Figure 3. Full XPS spectra (a) and V2p XPS spectra (b) of the LVP/C products

Different milling dispersants may lead to different dispersion uniformity of the raw materials, especially of the pyrolytic carbon converted from sucrose in the precursors, which will ultimately influence the microscopic structure and morphology of the final products. In order to disclose the effect and the underlying disciplines, several techniques including SEM, TEM, particle size detection and carbon content analysis were used combinedly. Fig. 4 shows the SEM images of the LVP/C samples synthesized with different ball-milling dispersants. As can be seen from Fig. 4, the dispersants used in the ball mill process affect the particle size and agglomeration state of the samples. The most obvious agglomeration is observed for the sample with Vethanol:Vwater=1:1, while the particles are the smallest and distribute the most uniformly for the sample with Vethanol:Vwater=1:0. More accurate and quantified results are further provided by the particle size tests.



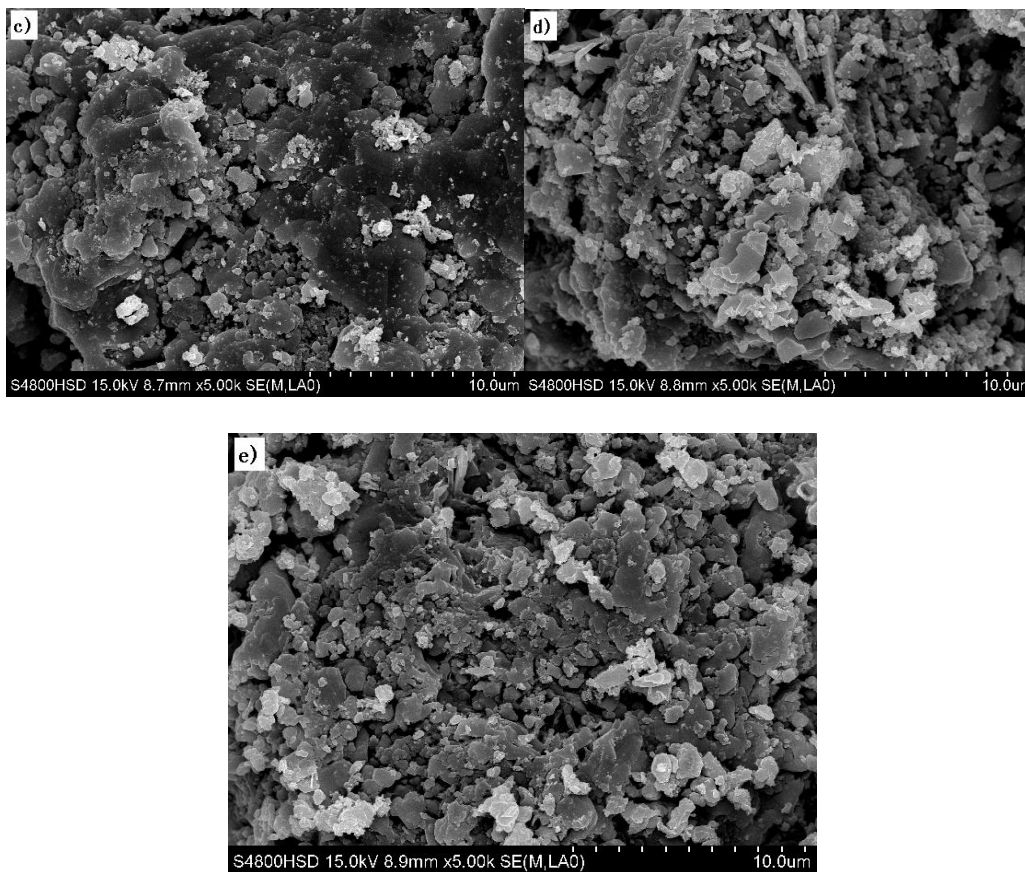


Figure 4. SEM images of the LVP/C composites synthesized with different ball-milling dispersants a) Vethanol:Vwater=0:1, b) Vethanol:Vwater=1:3, c) Vethanol:Vwater=1:1, d) Vethanol:Vwater=3:1, e) Vethanol:Vwater=1:0

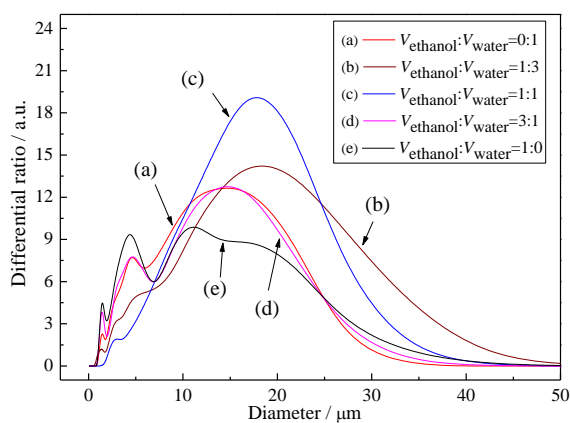


Figure 5. Particle size distribution of the LVP/C composites synthesized with different ball-milling dispersants

The particle size distribution curves are given in Fig. 5, and the corresponding D50 values are listed in Table 2. Fig. 5 shows that when pure ethanol is used as dispersant (Vethanol:Vwater=1:0), the minimum D50 value of 6.47μm is reached. With the decrease in the used amount of ethanol, the

particle size increases first and then decreases. When pure water is used as dispersant ($V_{\text{ethanol}}:V_{\text{water}}=0:1$), the D50 value is $8.49\mu\text{m}$.

Table 2. D50 value and carbon content of the LVP/C composites synthesized with different ball-milling dispersants

$V_{\text{ethanol}}:V_{\text{water}}$	0:1	1:3	1:1	3:1	1:0
D_{50} (μm)	8.49	12.22	13.00	8.37	6.47
carbon content (mass%)	3.38	1.53	3.11	3.36	4.63

The TEM images are further employed to examine the carbon layers encapsulating the LVP particles, as shown in Fig. 6. When pure ethanol is used as dispersant ($V_{\text{ethanol}}:V_{\text{water}}=1:0$), the carbon layer is about 50nm thick, and distributed relatively evenly. When pure water is used as dispersant ($V_{\text{ethanol}}:V_{\text{water}}=0:1$), the carbon layer is about 30nm thick. Table 2 list the carbon content in the as-synthesized LVP/C samples with different dispersants. Among them, when $V_{\text{ethanol}}:V_{\text{water}}=1:0$, the carbon content of the obtained LVP/C sample is up to 4.63%. With the decreases of the amount of ethanol in dispersion agent, the carbon content decreases first and then increases. When $V_{\text{ethanol}}:V_{\text{water}}=0:1$, the carbon content is 3.38%. From the above results, it is found that there is a certain relationship between the carbon content and D50 values of the particle size distribution, that is, the larger the carbon content, the smaller the particle size (Table 2 and Fig. 5). A reasonable interpretation may be that the carbon layer may restrict the growth of LVP grains and agglomeration of the LVP/C particles.

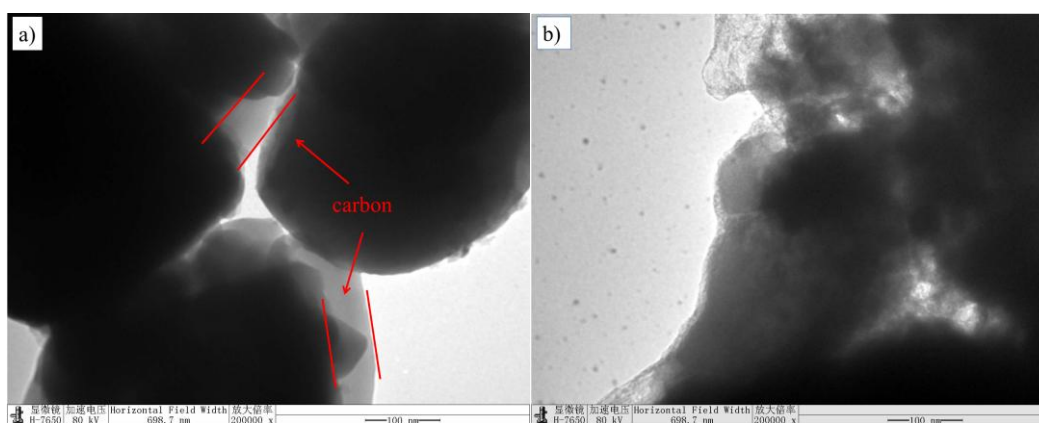


Figure 6. TEM images of the LVP/C composites synthesized with different ball-milling dispersants a) $V_{\text{ethanol}}:V_{\text{water}}=0:1$ and b) $V_{\text{ethanol}}:V_{\text{water}}=1:0$

3.2 Effect of ball-milling dispersants on the electrochemical properties of the LVP/C composites

Fig. 7 shows the CV curves of the LVP/C samples synthesized with different ball-milling dispersants. All samples exhibit three pairs of oxidation/reduction peaks and the position of peak

potential changes little around 3.65V/3.55V, 3.71V/3.61V and 4.12V/4.01V. Table 3 is a comparison of peak potential separations (ΔE_p) of the synthesized LVP/C samples. Table 3 shows that when pure water or ethanol is used as milling dispersant, ΔE_p are markedly less than those of the other three samples, indicating the best electrode process reversibility and least ohmic resistance.

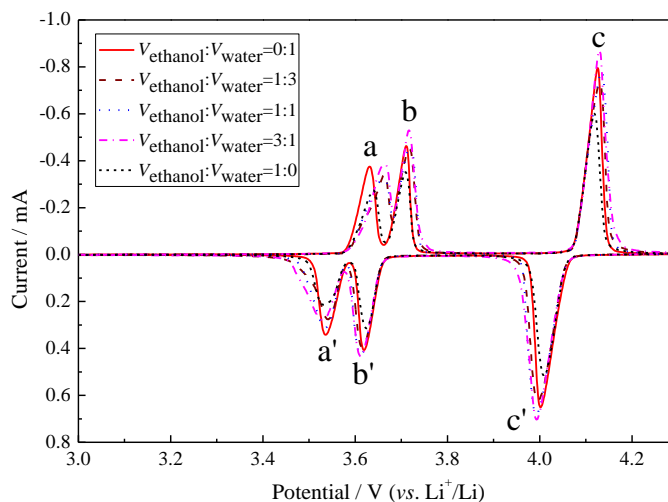


Figure 7. CV curves of the synthesized LVP/C composites (scan rate is 0.1 mV s^{-1})

Table 3. Peak potential separations (ΔE_p) between cathodic and anodic peaks

$V_{\text{ethanol}}:V_{\text{water}}$	0:1	1:3	1:1	3:1	1:0
ΔE_p of peaks a/a' (mV)	95	123	126	137	107
ΔE_p of peaks b/b' (mV)	92	102	107	105	84
ΔE_p of peaks c/c' (mV)	124	134	141	137	108

In order to examine the cycling performance of the LVP/C samples, galvanostatic charge and discharge tests were conducted at 1C and 10C rates. The LVP/C cathodes were assembled into CR2025-type coin cells with lithium sheets as reference and counter electrodes, and the charge and discharge cut-off voltages are 4.3V and 3.0V, and the charge and discharge rates are 1C and 10C, respectively. Fig. 8 shows the cycle life curves of the LVP/C composites prepared with different ball-milling dispersants at 1C rate. When $V_{\text{ethanol}}:V_{\text{water}}=1:0$, the initial discharge specific capacity of the synthesized LVP/C sample is the highest and reaches 122.5 mAh g^{-1} , which is 92.2% of the theoretical specific capacity, and the capacity retention is 97.3% after 100 cycles. When $V_{\text{ethanol}}:V_{\text{water}}=0:1$, the initial discharge specific capacity is 119.6 mAh g^{-1} , which is 89.9% of the theoretical specific capacity, and the capacity retention is 98.4% after 100 cycles. Comparatively, the capacities of the other samples are markedly lower. Fig. 9 shows the cycle life curves of the LVP/C composites prepared with

different ball-milling dispersants at 10C rate. When Vethanol:Vwater=1:0, the initial discharge capacity of the synthesized LVP/C sample is 106.0mAh g⁻¹ and the capacity retention is 95.2% after 100 cycles. When Vethanol:Vwater=0:1, the initial discharge capacity is 106.4mAh g⁻¹ and the capacity retention is 96.6% after 100 cycles. Therefore, when charged and discharged at high rate (10C), the synthesized LVP/C samples with Vethanol:Vwater=0:1 and Vethanol:Vwater=1:0 deliver almost the same discharge capacities, while the electrochemical properties of the other samples are rather poor. Compared with the results in literature, e.g. for LVP synthesized with ethanol or acetone as ball-milling dispersant [16-19], the specific capacities at 1C and 10C rates of the sample synthesized with Vethanol:Vwater=0:1 as ball-milling dispersant are comparable or even better.

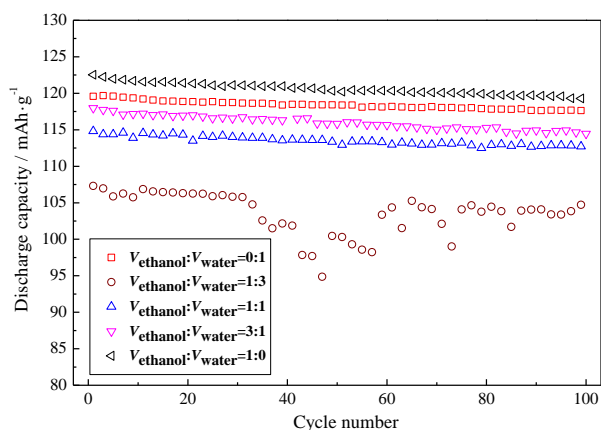


Figure 8. Cycling performances of the LVP/C composites synthesized with different ball-milling dispersants at 1C rate.

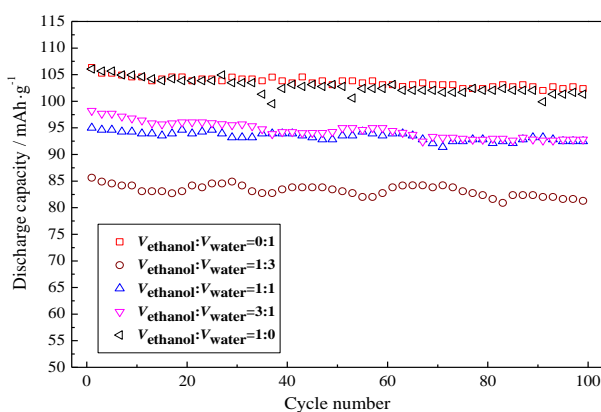


Figure 9. Cycling performances of the LVP/C composites synthesized with different ball-milling dispersants at 10C rate.

From the above tests, it can be concluded that the LVP/C samples synthesized with Vethanol:Vwater=0:1 and Vethanol:Vwater=1:0 possess a higher discharge capacity and stable cycling performance. Therefore, higher rate capabilities of the two LVP/C materials were further examined. Because large charging current causes large polarization, the charging voltage plateau will shift higher.

Therefore, we made some adjustments for the experimental test steps: first, the cell is charged at 20C rate until a cut-off voltage of 4.5V, and then charged at a constant voltage of 4.3V for a period of time, finally, discharged at 20C to a cut-off voltage of 3.0V. Fig. 10 shows the cycle life curves of the LVP/C samples synthesized with pure ethanol ($V_{\text{ethanol}}:V_{\text{water}}=0:1$) and water ($V_{\text{ethanol}}:V_{\text{water}}=1:0$) as ball-milling dispersants at 20C rate. It can be seen that the maximum discharge capacities of the LVP/C samples synthesized with pure ethanol ($V_{\text{ethanol}}:V_{\text{water}}=0:1$) and water ($V_{\text{ethanol}}:V_{\text{water}}=1:0$) are 98.2 mAh g^{-1} and 96.8 mAh g^{-1} , and the capacity retentions are 95.7% and 98.5% after 100 cycles, respectively. Therefore, both the samples exhibit good high-rate performances.

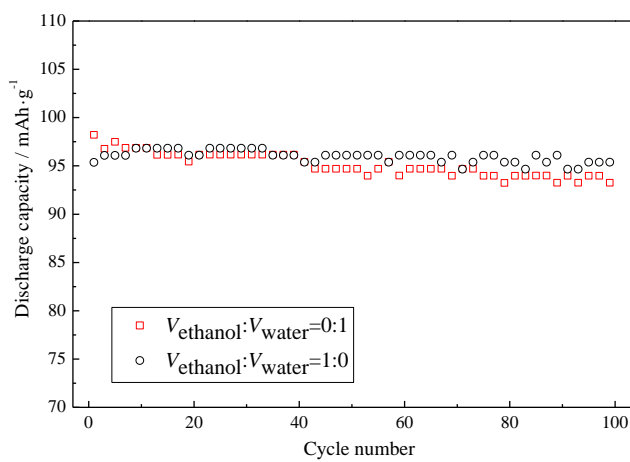


Figure 10. Cycling performances of the LVP/C composites synthesized with different ball-milling dispersants at 20C rate

From the above experimental results, we can know that the various ball-milling dispersants exert different influences on the structure, morphology and electrochemical performances of the as-synthesized LVP/C composite materials. The choice of pure ethanol or water as ball-milling dispersant can produce uniform carbon coating layer with adequate thickness avoiding excessive growth of LVP grains and agglomeration of LVP/C particles, which retains good electronic conductivity as well as electrochemical reactivity. Although the LVP/C samples synthesized with $V_{\text{ethanol}}:V_{\text{water}}=0:1$ delivers a slightly lower discharge capacity at low rate than that for the sample synthesized with $V_{\text{ethanol}}:V_{\text{water}}=1:0$, the electrochemical performances of both the samples at high rates are comparable. This makes using water as ball milling dispersant feasible in industrial production.

3.3 The determination of the Li^+ ion diffusion coefficient of the as-synthesized LVP/C composites

The lithium ion diffusion process in solid phase is usually one of the rate-determining steps for lithium-intercalated electrode materials. Therefore, the lithium ion diffusion coefficient, representing the velocity of the solid-phase diffusion, is an important parameter affecting high rate capability.

3.3.1 The Li^+ ion diffusion coefficient of the LVP/C composites determined with CV method

Fig. 11 shows the CV curves of the LVP/C composites synthesized with pure water (the sample is denoted as LVP-W) and pure ethanol (LVP-E) as ball-milling dispersant at different scan rates, and the peak potential separations between anodic and cathodic peaks, ΔE_p , at different scan rates are measured from the CV curves in Fig. 11 and listed in Table 4. It is observed that the peak potential separations of peaks b/b' and c/c' for LVP-E are less than those for LVP-W, which indicates that the electrode process reversibility of LVP-E is superior to that of LVP-W.

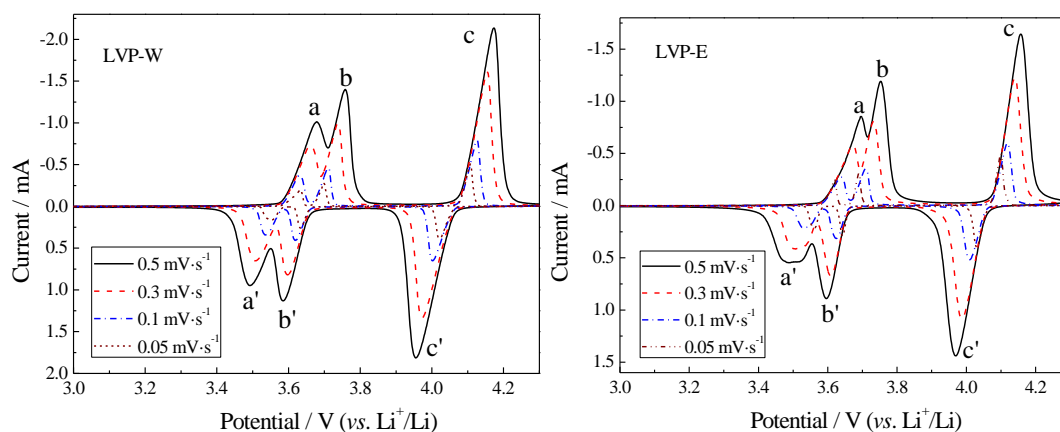


Figure 11. CV curves of the LVP/C composites at different scan rates

Table 4. Peak potential separations (ΔE_p) of the LVP/C composites at different scan rates

Samples	LVP-W				LVP-E			
	0.5	0.3	0.1	0.05	0.5	0.3	0.1	0.05
Scan rate (mV s^{-1})	0.5	0.3	0.1	0.05	0.5	0.3	0.1	0.05
ΔE_p of peaks a/a' (mV)	185	154	95	80	209	165	107	59
ΔE_p of peaks b/b' (mV)	172	140	92	65	156	123	85	48
ΔE_p of peaks c/c' (mV)	218	182	124	86	190	153	109	70

According to the classical Randles Sevcik equation, the peak current should be proportional to the square root of the scan rate, as expressed by Equation (1),

$$I_p = 2.69 \times 10^5 n^{3/2} A D_{\text{Li}^+}^{1/2} C_{\text{Li}^+} v^{1/2} \quad (1)$$

where I_p is the peak current (A); n is the number of electrons per reaction species; A is the electrode/electrolyte interface area (cm^2), and here adopts the geometric area of the electrode and is 1.5394 cm^2 ; D_{Li^+} is the lithium ion diffusion coefficient in the solid phase of LVP ($\text{cm}^2 \text{ s}^{-1}$); C_{Li^+} is the concentration of lithium ions in the solid phase of LVP ($\text{mol}\cdot\text{cm}^{-3}$); and ν is the potential scan rate ($\text{V}\cdot\text{s}^{-1}$).

The calculation method of C_{Li^+} is the moles of Li per unit cell divided by the volume of unit cell. First, there are 12 Li^+ in each unit cell of LVP, and the unit cell volume can be obtained by XRD analysis, as shown in Table 1. Therefore, the Li^+ concentration in completely lithiated LVP solid phase can be calculated. Secondly, at the first pair of redox peaks (a/a'), 0.5 lithium ions are extracted from each LVP molecule, i.e., 2 Li^+ are extracted from each unit cell and 10 Li^+ are left in each unit cell. At the second pair of redox peaks (b/b'), another 2 Li^+ are extracted from each unit cell and 8 Li^+ are left in each unit cell. At the third pair of redox peaks (c/c'), 4 Li^+ are extracted from each unit cell and 4 Li^+ are left in each unit cell. Thus, the Li^+ solid phase concentration in LVP at different intercalated states can be calculated and are listed in Table 5.

Table 5. Solid phase concentration of Li^+ in LVP at different intercalated states ($\text{mol}\cdot\text{cm}^{-3}$)

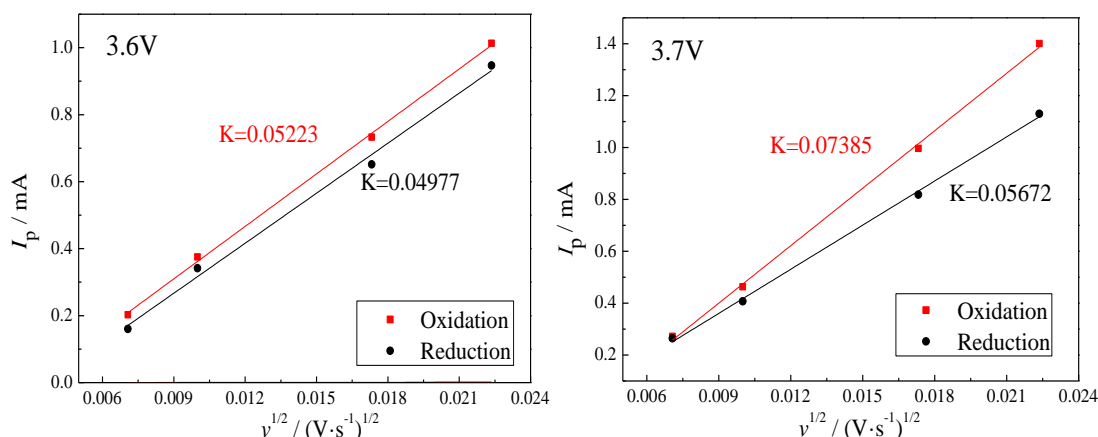
Samples	LVP-W	LVP-E
C_{Li^+} in $\text{Li}_{3.0}\text{V}_2(\text{PO}_4)_3$	2.24606×10^{-2}	2.258913×10^{-2}
C_{Li^+} in $\text{Li}_{2.5}\text{V}_2(\text{PO}_4)_3$	1.871716×10^{-2}	1.882428×10^{-2}
C_{Li^+} in $\text{Li}_{2.0}\text{V}_2(\text{PO}_4)_3$	1.497373×10^{-2}	1.505942×10^{-2}
C_{Li^+} in $\text{Li}_{1.0}\text{V}_2(\text{PO}_4)_3$	0.748687×10^{-2}	0.752971×10^{-2}

We define

$$K = 2.69 \times 10^5 n^{3/2} A D_{\text{Li}^+}^{1/2} C_{\text{Li}^+} \quad (2)$$

then, equation (1) can be rewritten as,

$$I_p = K \nu^{1/2} \quad (3)$$



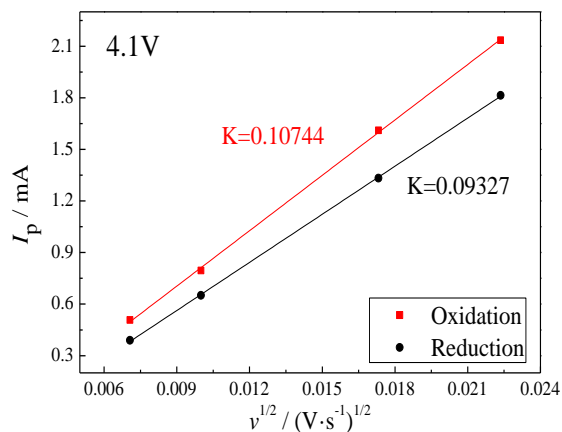


Figure 12. I_p as the function of $v^{1/2}$ for the LVP-W sample

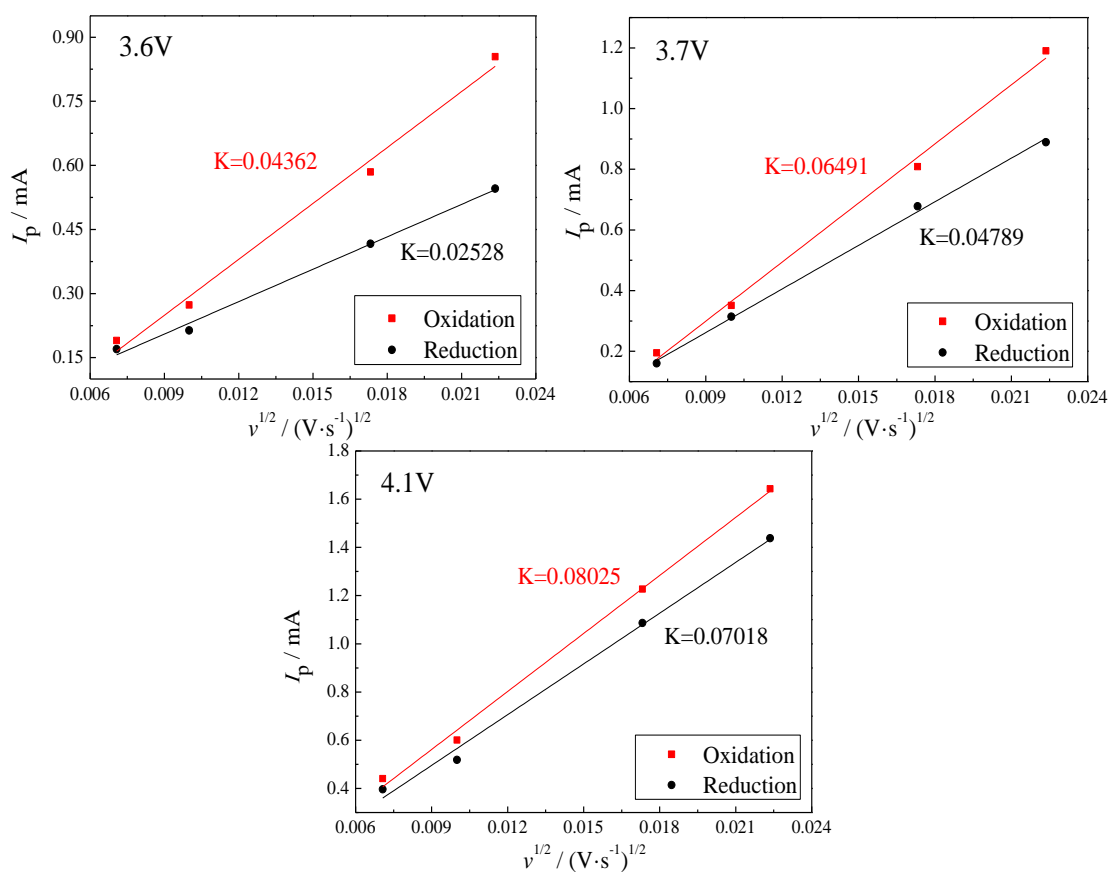


Figure 13. I_p as the function of $v^{1/2}$ for the LVP-E sample

The relationship curves of I_p vs. $v^{1/2}$ at different redox peaks for the LVP-W and LVP-E samples are presented in Fig. 12 and 13, respectively, and the linearity of these curves confirms the diffusion-limited behavior. According to equation (2), the lithium ion diffusion coefficients are calculated from the slope (K) of the lines, as summarized in Table 6. These values are at the same order of magnitude as those determined with CV method in literature [20, 21].

Table 6. Lithium ion diffusion coefficients at different peaks for the two samples ($\text{cm}^2 \cdot \text{s}^{-1}$)

Stage discription		LVP-W	LVP-E
Oxidation/charge	Peak a	2.5228×10^{-10}	1.7396×10^{-10}
	Peak b	7.2628×10^{-10}	5.5471×10^{-10}
	Peak c	3.0024×10^{-10}	1.6560×10^{-10}
Reduction/discharge	Peak a'	3.2987×10^{-10}	8.4139×10^{-11}
	Peak b'	6.6941×10^{-10}	4.7180×10^{-10}
	Peak c'	9.0506×10^{-10}	5.0660×10^{-10}

Table 6 shows that the values of D_{Li^+} for LVP-E and LVP-W are both at the order of $10^{-10} \text{cm}^2 \cdot \text{s}^{-1}$ and follow the same variation tendency during the charging and discharging processes. For the charging process, it can be seen that with lithium ion removing, Li^+ diffusion coefficient becomes larger and then smaller. This is because the reduction of Li^+ ions in the lattice benefits the Li^+ diffusion in the three-dimensional channels, but further extraction of Li from Li-deficient $\text{Li}_2\text{V}_2(\text{PO}_4)_3$ at peak c turns difficult. While for the discharging process, lack of Li in the lattice facilitates the diffusion in the three-dimensional channels as well as the reintercalation of Li into the lattice, therefore, D_{Li^+} at peak c' is the largest, followed by at peak b' and a'.

Another important phenomenon is that the values of D_{Li^+} for LVP-W at different stages are all larger than those for LVP-E, and this is probably the reason why the specific capacity of LVP-W is almost the same as that of LVP-E at high rates (10C and 20C, in Fig. 9 and 10), although it's smaller than LVP-E at low rate (1C, in Fig. 8). At 1C rate, the smaller capacity of LVP-W is caused by the difference in electronic conductivity due to less carbon coating amount, while at high rates, the effect of Li^+ diffusion in LVP solid phase is more predominant.

3.3.2 The Li^+ ion diffusion coefficient of the LVP/C composites determined with EIS method.

It is well known that EIS plots can provide the information of various basic electrode processes in different frequency ranges, including that of diffusion process. Fig. 14 shows EIS Nyquist plots of the two electrode materials at different state of charge. Here state of charge (SoC) is actually equivalent to the degree of delithiation and 100% of state of charge corresponds to the removal of 2 Li^+ from a LVP molecule.

The Li^+ ion diffusion coefficient of the LVP/C composites can be determined according to equation (4),

$$D_{\text{Li}^+} = \frac{R^2 T^2}{2n^4 F^4 A^2 C_{\text{Li}^+} \sigma} \quad (4)$$

where D_{Li^+} is the lithium ion diffusion coefficient in the solid phase of LVP ($cm^2 s^{-1}$); R is the gas constant and is $8.314 J K^{-1} mol^{-1}$; T is the absolute temperature and here is $293.15 K$; n is the valence state of the diffusion species and here is 1 for Li^+ ; F is Faraday constant and is $96485 C mol^{-1}$; A is the electrode/electrolyte interface area (cm^2), and here adopts the geometric area of the electrode and is $1.5394 cm^2$; C_{Li^+} is the concentration of lithium ions in the solid phase of LVP ($mol cm^{-3}$); σ is Warburg coefficient ($\Omega^{-1} s^{1/2}$).

σ can be obtained from the slopes of the plots of impedance real part Z' and the reciprocal of the square root of angular frequency in diffusion region at low frequencies, as shown in Fig. 15, according to equation (5)

$$Z' = R_u + R_{ct} + \sigma \omega^{-1/2} \quad (5)$$

The calculated diffusion coefficients are depicted at different states of charge in Fig. 16. It is observed that the diffusion coefficients increase with the state of charge to the maximum at 80% SoC and then drop. This tendency is consistent with the diffusion coefficients of charging process obtained with CV methods (Table 6). Although the diffusion coefficients of LVP-W are slightly smaller than those of LVP-E at low SoCs, the maximum at 80% SoC is larger, indicating good lithium ion diffusion behavior.

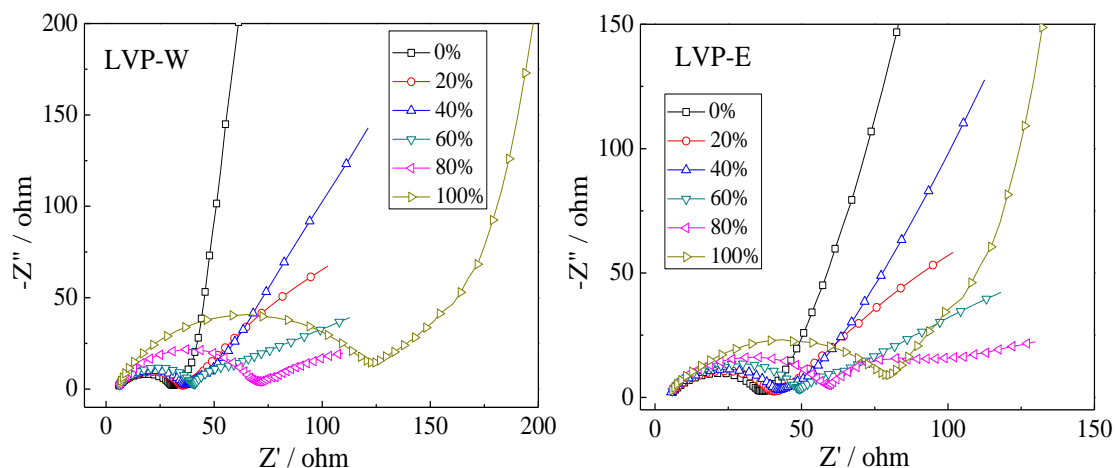


Figure 14. Nyquist plots of the LVP/C cathodes at different states of charge

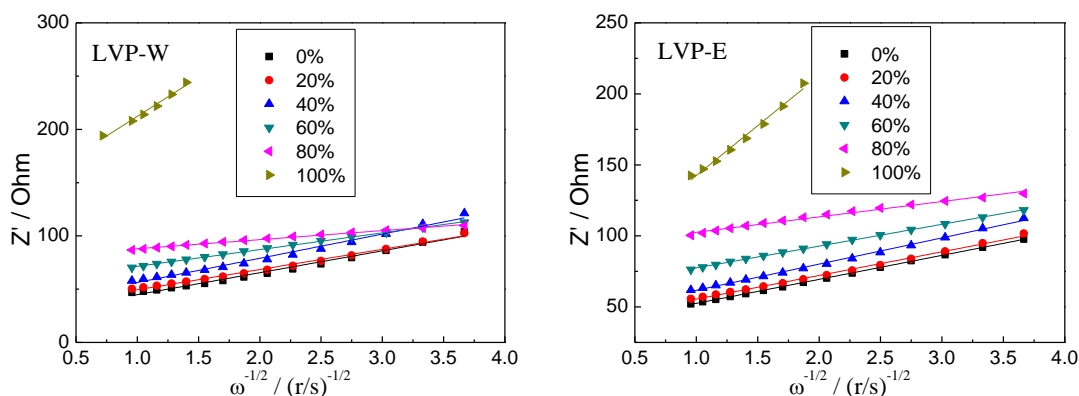


Figure 15. Relationship curves of Z' and $\omega^{-1/2}$ at different states of charge

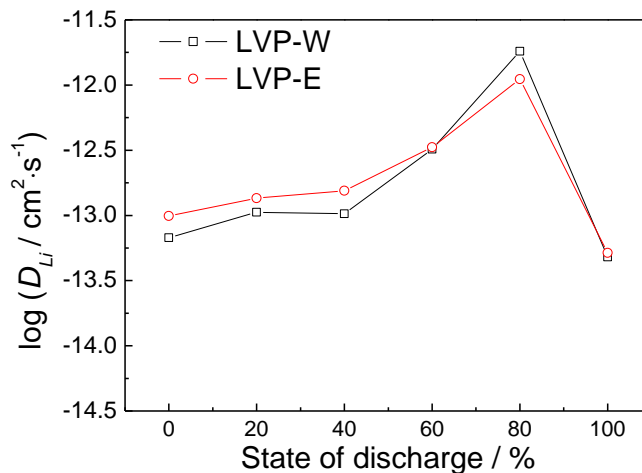


Figure 16. Li^+ diffusion coefficients in LVP at different states of charge.

4. CONCLUSION

In this paper, a series of LVP/C composites were synthesized with different ball-milling dispersants and the impacts of the dispersants on morphology and electrochemical performances of the as-synthesized samples were investigated systematically. The results show that the LVP/C samples synthesized with pure ethanol and pure water as dispersants have uniformly distributed carbon coating layers with adequate thickness and moderate particle size distribution, which facilitate the improvement of electronic conduction and electrochemical reactivity of the materials. The galvanostatic charge/discharge tests show that at 1C rate, the initial discharge capacities of the LVP/C samples synthesized with pure ethanol and water as dispersants reach 122.5mAh g^{-1} and 119.6mAh g^{-1} , respectively. These values are much larger than the other samples prepared with mixtures of ethanol and water as dispersants. At high rates (10C and 20C), the LVP/C samples synthesized with pure ethanol and water as dispersants deliver comparable discharge capacities and good cycling stability, indicating excellent high-rate capability. The lithium ion diffusion coefficients measured with CV method are of the order of magnitude of $10^{-10} \sim 10^{-11} \text{cm}^2 \text{s}^{-1}$, and the values of D_{Li^+} measured with EIS method are of the order of magnitude of $10^{-12} \sim 10^{-14} \text{cm}^2 \text{s}^{-1}$ for the LVP/C samples synthesized with pure ethanol and water as dispersants, indicating that they both have large lithium ion transport rates.

ACKNOWLEDGMENTS

This work was supported by the National Natural Science Foundation of China (Grant nos. 51274075), the National Environmental Technology Special Project (No. 201009028), and Guangdong Province-department University-industry Collaboration Project (Grant nos. 2012B091100315).

References

1. S.C. Yin, H. Grondey, P. Strobel, H. Huang and L.F. Nazar, *J. Am. Chem. Soc.*, 125 (2003) 326.
2. S.C. Yin, H. Grondey, P. Strobel, M. Anne and L.F. Nazar, *J. Am. Chem. Soc.*, 125 (2003) 10402.

3. H. Huang, S.C. Yin, T. Kerr, N. Taylor and L.F. Nazar, *Adv. Mater.*, 14 (2002) 1525.
4. L. Wang, L.C. Zhang, I. Lieberwirth, H.W. Xu and C.H. Chen, *Electrochem. Commun.*, 12 (2010) 52.
5. C.S. Dai, Z.Y. Chen, H.Z. Jin and X.G. Hu. *J. Power Source*, 195 (2010) 5775.
6. P. Fu, Y.M. Zhao, Y. Z. Dong, X.M. An and G.P. Shen, *J. Power Sources*, 162 (2006) 651.
7. Y.Q. Qiao, X.L. Wang, J.Y. Xiang, D. Zhang, W.L. Liu and J.P. Tu, *Electrochim. Acta*, 56 (2011) 2269.
8. X.J. Zhu, Y.X. Liu, L.M. Geng, L.B. Chen, H.X. Liu and M.H. Cao, *Solid State Ionics*, 179 (2008) 1679.
9. Y. Tang, B.H. Zhong, X.D. Guo, H. Liu, Y.J. Zhong, X. Nie and H. Tang, *Acta Phys. -Chim. Sin.*, 27(4) (2011) 869.
10. B.Q. Jiang, S.F. Hu and M.W. Wang, *Advanced Materials Research*, 156-157(2011) 1219.
11. X.H. Rui, C. Li and C.H. Chen, *Electrochim. Acta*, 54 (2009) 3374.
12. X.H. Rui, Y. Jin, X.Y. Feng, L.C. Zhang and C.H. Chen, *J. Power Sources*, 196 (2011) 2109.
13. Y.Q. Qiao, X.L. Wang, J.Y. Xiang, D. Zhang, W.L. Liu and J.P. Tu, *Electrochim. Acta*, 56 (2011) 2269.
14. X.C. Zhou, Y.M. Liu and Y.L. Guo, *Electrochim. Acta*, 54 (2009) 2253.
15. L.J. Wang, Z.Y. Tang, L. Ma and X.H. Zhang, *Electrochem. Commun.*, 13 (2011) 1233.
16. Y.Q. Qiao, J.P. Tu, Y.J. Mai, L.J. Cheng, X.L. Wang and C.D. Gu, *J. Alloy. Compd.* 509 (2011) 7181.
17. P. Fu, Y.M. Zhao, Y.Z. Dong, X.N. An and G.P. Shen, *Electrochim. Acta* 52 (2006) 1003.
18. X.C. Zhou, Y.M. Liu and Y.L. Guo, *Solid State Commun.* 146 (2008) 261.
19. P. Fu, Y.M. Zhao, Y.Z. Dong, X.N. An and G.P. Shen, *J. Power Sources* 162 (2006) 651.
21. X.H. Rui, N. Ding, J. Liu, C. Li and C.H. Chen, *Electrochim. Acta* 55 (2010) 2384.
22. X.H. Rui, N. Yesibolati, S.R. Li, C.C. Yuan and C.H. Chen, *Solid State Ionics* 187 (2011) 58.